Parametric and nonparametric magnetic response enhancement via electrically induced magnetic moments

Bastian Jungnitsch* and Jörg Evers†
Max-Planck-Institut für Kernphysik, Saupfercheckweg 1, D-69117 Heidelberg
(Received 22 April 2008; revised manuscript received 25 July 2008; published 16 October 2008)

The realization of negative refraction in atomic gases requires a strong magnetic response of the atoms. Current proposals for such systems achieve a parametric enhancement of the magnetic response by one inverse power of the fine-structure constant α, but still rely on high gas densities. To enable further enhancement, here we study in detail the magnetic and electric response to a probe field interacting with three-level atoms in ladder configuration. In our first model, the three transitions are driven by a control field and the electric and magnetic components of the probe field, giving rise to a closed interaction loop. In a reference model, the coherent driving is replaced by an incoherent pump field. A time-dependent analysis of the closed-loop system enables us to identify the different contributions to the medium response and to determine the enhancement mechanism. Based on these results, we show that in addition to the parametric enhancement of $\alpha^{-1} \sim 137$, our system allows for a further nonparametric enhancement of the magnetic response by almost two orders of magnitude, relaxing the requirement for a high vapor density.

DOI: 10.1103/PhysRevA.78.043817 PACS number(s): 42.50.Gy, 42.65.Sf, 42.65.An, 32.80.Wr

I. INTRODUCTION

As Veselago pointed out in 1968, materials having both negative permittivity and negative permeability can acquire a negative index of refraction [1,2]. Such negative index materials are also called "left-handed," since the electric ($\vec{E}$) and magnetic ($\vec{H}$) components of an electromagnetic wave traveling through a negatively refracting medium and its wave vector form a left-handed coordinate system. These materials offer promising applications [2–4], such as the possibility to overcome the diffraction limit with a negatively refracting, perfect lens, as proposed by Pendry [5]. Therefore it is not surprising that, in the recent past, left-handed materials and negative refraction have been studied intensely. These efforts have been fueled by a multitude of successful experimental demonstrations of negative refraction and related effects, mostly relying on metamaterials [6–11]. Metamaterials are artificial structures with feature size below the incident radiation wavelength that allow the electromagnetic response to be controlled to a great extent and at the same time appear as a bulk medium to the incident radiation.

A different ansatz is the quantum optical realization of negative refraction in dense atomic gases [12–15]. Negative refraction, however, typically requires both electric and magnetic response at the probe field frequency, which is hampered by the fact that usually the coupling of the magnetic component of a probe laser field to a magnetic dipole transition in atoms is strongly suppressed. A simple order-of-magnitude estimate shows that the suppression factor is proportional to two powers of the fine-structure constant, $\alpha^2 \sim 137^{-2}$. Thus, additional effort is required in order to enhance the magnetic response. In the literature, a number of schemes that allow to achieve a high positive index of refraction with small absorption have been proposed. They are based on a suitable modification of the electric response of the medium (see, e.g., [16]). The enhancement, however, is typically too small such that a direct transfer of these ideas to magnetic transitions is not straightforward.

Thus, the schemes suggested so far for negative refraction rely on a different mechanism that is related to an enhancement via chirality [12,14,15,17]. The medium is such that the magnetic response is influenced by both the electric and the magnetic component of the probe field and analogously for the electric response. In essence, this allows to achieve a parametric enhancement of the magnetic response by one inverse power of the fine-structure constant. A first interpretation for the case of atomic systems has been given in [12], which, however, did not consider the coupling of the magnetic probe field component to the atomic system in deriving the induced magnetic dipole moment. It also focused on the so-called multiphoton resonance case for the applied fields and the employed level structure such that the enhancement could only be predicted for a single probe field frequency. In contrast, subsequent work reported an enhancement via chiral contributions over a range of probe field frequencies [14,15]. Nevertheless, more insight into the exact mechanism of the parametric enhancement via chiral contributions is desirable, not least since it might enable one to further enhance the magnetic response, for example, via nonparametric enhancements independent of the fine-structure constant.

Motivated by this, here we study in detail the enhancement mechanism that is at the heart of current schemes to achieve negative refraction in atomic gases, and achieve two main results. First, in a time-dependent analysis beyond the multiphoton resonance condition used in previous studies, we identify the physical mechanism leading to the chiral enhancement. Second, we show that in addition to the parametric chiral enhancement by $\alpha^{-1} \sim 137$, our system can exhibit a nonparametric enhancement of order 10^2, such that the total enhancement of the magnetic response is almost of order α^{-2}. Such a combination of parametric and nonpara-

*bastian.jungnitsch@mpi-hd.mpg.de
†joerg.evers@mpi-hd.mpg.de

metric enhancement could enable negative refraction in atomic gases at substantially lower densities, thereby facilitating the experimental realization.

For this, we reconsider the three-level ladder-type system studied in [12], where one transition is driven by a coherent control field and the other two transitions couple to the magnetic and electric component of a probe field. In contrast to previous studies, we apply a time-dependent analysis of the medium response that enables us to directly identify the various physical processes contributing to the medium response. These results are compared to a reference system that is obtained by replacing the coherent driving field by an incoherent pumping field. We find that the enhancement of the magnetic response occurs since the used level schemes are so-called closed-loop media. In these systems, the laser fields applied are such that they form a closed interaction loop. We identify the scattering process giving rise to the chiral enhancement of the magnetic response as a scattering of the coupling field and of the electric probe field component into the magnetic probe field component and provide conditions for this process to take place. Our results explain why, in the studied three-level systems, the enhancement only occurs at a single probe field frequency, while in larger level schemes, the laser fields can be applied in such a way that the enhancement works at arbitrary frequencies of the probe field. Also, we show that enhancement is possible only for coherently driven systems.

From our time-dependent analysis, we also obtain an analytic expression for the chiral scattering contribution giving rise to the parametric enhancement by α^{-1}. An optimization of the control field parameters allows us to achieve a further nonparametric enhancement of the magnetic response by almost two orders of magnitude, which could significantly relax the stringent conditions on the vapor particle density.

The paper is organized as follows. In Sec. II, we present our model systems and derive the equations of motion as well as expressions for the medium response coefficients. In Sec. III, we solve the equations of motion, in the time-dependent case for the closed-loop configuration, for the time-independent case at multiphoton resonance, and in the incoherently pumped system. Using these results, in Sec. IV we compare the different systems, identify the chiral enhancement mechanism, and show that further nonparametric enhancement is possible. Section V discusses and summarizes the results.

II. THEORETICAL CONSIDERATIONS

A. Model

We start by writing down the applied electromagnetic fields as shown in Fig. 1. Since we treat both systems semiclassically, we have

$$\vec{E}(\vec{r},t) = \vec{E}_p(\vec{r})e^{i\phi}e^{-i\omega_p t} + \vec{E}_c(\vec{r})e^{i\psi}e^{-i\omega_c t} + \text{c.c.}, \tag{1a}$$

$$\vec{B}(\vec{r},t) = \vec{B}_p(\vec{r})e^{i\phi}e^{-i\omega_p t} + \vec{B}_c(\vec{r})e^{i\psi}e^{-i\omega_c t} + \text{c.c.}, \tag{1b}$$

where the subscript p (c) refers to the probe (control) field. Further, $\vec{E}_p(\vec{r}) = \mathcal{E}_p\vec{e}_p e^{i\vec{k}_p\cdot\vec{r}}$, where $\mathcal{E}_p$ is the electric field amplitude, $\vec{e}_p$ the unit polarization vector of the electric component of the probe field, $\vec{k}_p$ the probe field's wave vector, ω_p its frequency, and ϕ its absolute phase. Analogously, $\vec{E}_c(\vec{r}) = \mathcal{E}_c\vec{e}_c e^{i\vec{k}_c\cdot\vec{r}}$, where $\mathcal{E}_c$ is the control field amplitude and $\vec{e}_c$ its unit polarization vector. $\vec{k}_c$ is the wave vector of the control field, ω_c its frequency, and ψ the control field's total phase. The magnetic probe field component is defined analogously as $\vec{B}_p(\vec{r}) = \mathcal{B}_p\vec{b}_p e^{i\vec{k}_p\cdot\vec{r}}$. Note that the magnetic probe field component unit polarization vector is $\vec{b}_p = \vec{\kappa}\times\vec{e}_p$ with unit propagation direction vector $\vec{\kappa} = \vec{k}_p/k_p$.

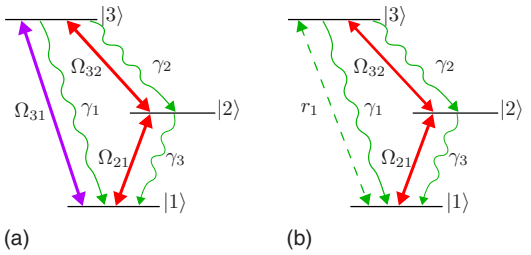

FIG. 1. (Color online) (a) Three-level system driven by coherent fields in loop configuration. The probe field components Ω_{21} and Ω_{32} are denoted by red solid double arrows, the coupling field Ω_{31} by purple solid double arrows. Spontaneous emission is indicated by the wiggly green arrows. The transition $|1\rangle \leftrightarrow |2\rangle$ couples to the magnetic component, while transition $|2\rangle \leftrightarrow |3\rangle$ couples to the electric component of the same probe field. (b) Reference system obtained by replacing the coherent control field by an incoherent, bidirectional pumping, indicated by the green dashed double arrow.

In the rotating-wave and dipole approximation, we arrive at the Hamiltonian

$$H = H_0 + H_I, \tag{2a}$$

$$H_0 = \sum_{j=1}^{3} \hbar\omega_j |j\rangle\langle j|, \tag{2b}$$

$$H_I = -\hbar(\Omega_{21}e^{-i\omega_p t}|2\rangle\langle 1| + \Omega_{32}e^{-i\omega_p t}|3\rangle\langle 2| + \Omega_{31}e^{-i\omega_c t}|3\rangle\langle 1| + \text{H.c.}). \tag{2c}$$

Note that, in the rotating-wave approximation, the magnetic control field component can be neglected, because it does not couple near-resonantly to a magnetic transition. In Eqs. (2), the energy of state $|i\rangle$ is $\hbar\omega_i$ ($i \in \{1,2,3\}$) and the Rabi frequencies are defined as

$$\Omega_{21} = e^{i\phi}\vec{B}_p(\vec{r})\vec{\mu}_{21}/\hbar, \tag{3a}$$

$$\Omega_{32} = e^{i\phi}\vec{E}_p(\vec{r})\vec{d}_{32}/\hbar, \tag{3b}$$

$$\Omega_{31} = e^{i\psi}\vec{E}_c(\vec{r})\vec{d}_{31}/\hbar. \tag{3c}$$

The electric dipole moments are defined as $\vec{d}_{32} = \langle 3|\vec{d}|2\rangle$ and $\vec{d}_{31} = \langle 3|\vec{d}|1\rangle$. Analogously, the magnetic dipole moment is $\vec{\mu}_{21} = \langle 2|\vec{\mu}|1\rangle$. Here, $\vec{d}$ and $\vec{\mu}$ are the electric and magnetic dipole operators, respectively, and $\vec{d}_{ij} = \vec{d}_{ji}^*$, $\vec{\mu}_{ij} = \vec{\mu}_{ji}^*$, and $\Omega_{ij} = \Omega_{ji}^*$.

B. Equations of motion

In this section, we derive the equations of motion for a general system that contains both systems of interest shown in Fig. 1 as special cases. To this end, we consider a three-level system that—on transition $|1\rangle \leftrightarrow |2\rangle$—combines coherent pumping by a control field and bidirectional incoherent pumping. Since this system is a closed-loop system, in general there is no stationary state in the long-time limit and the Hamiltonian necessarily has an intrinsic explicit time dependence [18–31]. To simplify this time dependence, we apply the transformation

$$V = e^{(i/\hbar)(H_0+X)t}(H_I - X)e^{-(i/\hbar)(H_0+X)t}, \tag{4}$$

where $X=\Delta_1|1\rangle\langle 1|+\Delta_2|2\rangle\langle 2|$. Here, we chose the notations $\Delta_1=\omega_3-\omega_1-\omega_c$ and $\Delta_2=\omega_3-\omega_2-\omega_p$ for the detunings. By applying this transformation, we arrive at the following equations of motions, if we include spontaneous decay in the Born-Markov approximation:

$$\frac{\partial}{\partial t}\tilde{\varrho}_{11} = -r_1\tilde{\varrho}_{11} + \gamma_3\tilde{\varrho}_{22} + (\gamma_1 + r_1)\tilde{\varrho}_{33} + ie^{-i\Delta t}\Omega_{12}\tilde{\varrho}_{21} - ie^{i\Delta t}\Omega_{21}\tilde{\varrho}_{12} + i\Omega_{13}\tilde{\varrho}_{31} - i\Omega_{31}\tilde{\varrho}_{13}, \tag{5a}$$

$$\frac{\partial}{\partial t}\tilde{\varrho}_{12} = -\left(i(\Delta - \Delta_3) + \frac{1}{2}(r_1 + \gamma_3)\right)\tilde{\varrho}_{12} - i\Omega_{32}\tilde{\varrho}_{13} - ie^{-i\Delta t}\Omega_{12}(\tilde{\varrho}_{11} - \tilde{\varrho}_{22}) + i\Omega_{13}\tilde{\varrho}_{32}, \tag{5b}$$

$$\frac{\partial}{\partial t}\tilde{\varrho}_{13} = -\left(i(\Delta - \Delta_2 - \Delta_3) + \frac{1}{2}(2r_1 + \gamma_1 + \gamma_2)\right)\tilde{\varrho}_{13} - i\Omega_{13}(\tilde{\varrho}_{11} - \tilde{\varrho}_{33}) - i\Omega_{23}\tilde{\varrho}_{12} + ie^{-i\Delta t}\Omega_{12}\tilde{\varrho}_{23}, \tag{5c}$$

$$\frac{\partial}{\partial t}\tilde{\varrho}_{22} = -\gamma_3\tilde{\varrho}_{22} + \gamma_2\tilde{\varrho}_{33} - ie^{-i\Delta t}\Omega_{12}\tilde{\varrho}_{21} + ie^{i\Delta t}\Omega_{21}\tilde{\varrho}_{12} - i\Omega_{32}\tilde{\varrho}_{23} + i\Omega_{23}\tilde{\varrho}_{32}, \tag{5d}$$

$$\frac{\partial}{\partial t}\tilde{\varrho}_{23} = -\left(-i\Delta_2 + \frac{1}{2}(r_1 + \gamma_1 + \gamma_2 + \gamma_3)\right)\tilde{\varrho}_{23} - i\Omega_{13}\tilde{\varrho}_{21} + ie^{i\Delta t}\Omega_{21}\tilde{\varrho}_{13} + i\Omega_{23}(\tilde{\varrho}_{33} - \tilde{\varrho}_{22}), \tag{5e}$$

$$\tilde{\varrho}_{33} = 1 - \tilde{\varrho}_{11} - \tilde{\varrho}_{22}. \tag{5f}$$

Here, $\tilde{\varrho}_{ij}$ $(i,j\in\{1,2,3\})$ is the density matrix in the interaction picture obtained by transformation of ϱ_{ij} according to Eq. (4). One can see that this transformation simplifies the explicit time dependence on the right-hand side of the equations of motion to factors of $e^{\pm i\Delta t}$ in front of the weak magnetic probe field Rabi frequency Ω_{21} or Ω_{12}, respectively. γ_i are spontaneous emission rates on the different transitions. Also, we introduced the detuning on the magnetic probe field transition $\Delta_3=\omega_2-\omega_1-\omega_p$, as well as the so-called multiphoton detuning

$$\Delta = \Delta_2 + \Delta_3 - \Delta_1, \tag{6}$$

which for the current system evaluates to

$$\Delta = \omega_c - 2\omega_p. \tag{7}$$

By setting the incoherent pumping rate $r_1=0$ in Eqs. (5), we arrive at the equations of motion for the system in Fig. 1(a). Setting $\Omega_{31}=\Omega_{13}=\Delta=0$ yields the equations of motion for the incoherently pumped system shown in Fig. 1(b).

C. Electric and magnetic responses

Since our aim is to study the magnetic and electric responses, we require an expression for them in terms of the density matrix elements governed by Eqs. (5). We will find such a relation in this subsection. For this, it is important to note that electric fields can induce not only electric polarization, but also magnetization [14,17]. Similarly, magnetic fields can induce both magnetization and polarization.

For definitiveness, in the following we specialize to a circularly polarized (σ^+) probe field and probe field propagation in z direction, since one then obtains for the probe field polarization vectors $\vec{b}_p=-i\vec{e}_p$, i.e., they are parallel. Therefore, the tensorial structure of the response coefficients in the macroscopic polarization $\vec{P}$ and magnetization $\vec{M}$ simplifies considerably,

$$\vec{P}(\vec{r},t) = \frac{1}{c}\int_{-\infty}^{\infty}\xi_{EH}(\tau)\vec{H}(\vec{r},t-\tau)d\tau + \varepsilon_0\int_{-\infty}^{\infty}\chi_e(\tau)\vec{E}(\vec{r},t-\tau)d\tau, \tag{8a}$$

$$\vec{M}(\vec{r},t) = \frac{1}{c\mu_0}\int_{-\infty}^{\infty}\xi_{HE}(\tau)\vec{E}(\vec{r},t-\tau)d\tau + \int_{-\infty}^{\infty}\chi_m(\tau)\vec{H}(\vec{r},t-\tau)d\tau, \tag{8b}$$

and the electric and magnetic susceptibilities χ_e and χ_m and the chirality coefficients ξ_{HE} and ξ_{EH} become scalars. While the susceptibilities determine the electric (magnetic) response to the electric (magnetic) probe field component, the chiralities or cross terms determine the magnetic response to the electric probe field component, and vice versa. Here, c is the vacuum speed of light, and μ_0 and ε_0 are the vacuum permeability and permittivity. Note that, with the notation of Eqs. (8), the refractive index in Fourier space is given as [14]

$$n(\omega) = \sqrt{\tilde{\varepsilon}(\omega)\tilde{\mu}(\omega) - \frac{1}{4}[\tilde{\xi}_{EH}(\omega) + \tilde{\xi}_{HE}(\omega)]^2} + \frac{i}{2}[\tilde{\xi}_{EH}(\omega) - \tilde{\xi}_{HE}(\omega)], \tag{9}$$

where

$$\tilde{\varepsilon}(\omega) = \tilde{\chi}_e(\omega) + 1, \tag{10a}$$

$$\tilde{\mu}(\omega) = \tilde{\chi}_m(\omega) + 1, \tag{10b}$$

are the permittivity $\tilde{\varepsilon}(\omega)$ and the permeability $\tilde{\mu}(\omega)$ in Fourier space. Also, $\tilde{\xi}_{EH}(\omega)$, $\tilde{\xi}_{HE}(\omega)$, $\tilde{\chi}_m(\omega)$, and $\tilde{\chi}_e(\omega)$ are the Fourier-transformed response coefficients of the corresponding time domain quantities in Eqs. (8). They satisfy $\tilde{\chi}_e(\omega)^*$

$=\tilde{\chi}_e(-\omega)$, and similarly for the other susceptibilities and the chiralities. For vanishing chirality coefficients, Eq. (9) reduces to the well-known relation between the refractive index and the permittivity and permeability for nonchiral media [32].

Let us now continue to find an expression of the response coefficients in terms of the density matrix elements. Plugging Eqs. (1) into Eqs. (8), we arrive at

$$\vec{P} = \frac{\tilde{\xi}_{EH}(\omega_p)}{c\mu_0}\vec{B}_p(\vec{r})e^{i(\phi-\omega_p t)} + \frac{\tilde{\xi}_{EH}(\omega_c)}{c\mu_0}\vec{B}_c(\vec{r})e^{i(\psi-\omega_c t)} + \varepsilon_0\tilde{\chi}_e(\omega_p)\vec{E}_p(\vec{r})e^{i(\phi-\omega_p t)} + \varepsilon_0\tilde{\chi}_e(\omega_c)\vec{E}_c(\vec{r})e^{i(\psi-\omega_c t)} + \text{c.c.}, \tag{11a}$$

$$\vec{M} = \frac{\tilde{\xi}_{HE}(\omega_p)}{\mu_0 c}\vec{E}_p(\vec{r})e^{i(\phi-\omega_p t)} + \frac{\tilde{\xi}_{HE}(\omega_c)}{\mu_0 c}\vec{E}_c(\vec{r})e^{i(\psi-\omega_c t)} + \frac{1}{\mu_0}\tilde{\chi}_m(\omega_p)\vec{B}_p(\vec{r})e^{i(\phi-\omega_p t)} + \frac{1}{\mu_0}\tilde{\chi}_m(\omega_c)\vec{B}_c(\vec{r})e^{i(\psi-\omega_c t)} + \text{c.c.} \tag{11b}$$

Here, we have used $\vec{B}=\mu_0\vec{H}$, which strictly speaking only holds for microscopic local fields. Note that the Rabi frequencies in the equations of motion contain local fields, whereas Eqs. (8) contain macroscopic internal fields [15]. However, local field effects are not considered here and therefore we do not distinguish between internal and local fields, as is valid for moderate particle densities.

The polarization is also given by $\vec{P}=N\vec{p}$, and the magnetization by $\vec{M}=N\vec{m}$, where N is the particle density and $\vec{p}$ and $\vec{m}$ are the mean polarization and magnetization per atom [33]. We can express the mean polarization as $\vec{p}=\mathrm{Tr}(\varrho\vec{d})$ and the mean magnetization as $\vec{m}=\mathrm{Tr}(\varrho\vec{\mu})$. These traces can be written in terms of the transformed density matrix elements $\tilde{\varrho}_{ij}$ $(i,j\in\{1,2,3\})$ which are given as solutions of the equations of motion (5). If the light travels through the medium over a macroscopic distance, then the magnetic and electric response is determined by the part of the medium response that oscillates in phase with the probe field. In order to identify the relevant parts, we apply another unitary transformation into a system oscillating in phase with the probe field. We denote the density matrix in this frame by $\hat{\varrho}_{ij}$ $(i,j\in\{1,2,3\})$.

In the incoherently pumped system of Fig. 1(b), the Hamiltonian is time independent, and we find

$$\hat{\varrho}_{21} = \tilde{\varrho}_{21}, \tag{12a}$$

$$\hat{\varrho}_{32} = \tilde{\varrho}_{32}. \tag{12b}$$

On the other hand, in the closed-loop system of Fig. 1(a), the coherences $\hat{\varrho}_{32}$ and $\hat{\varrho}_{21}$ are given by

$$\hat{\varrho}_{21} = e^{i\omega_p t}\varrho_{21} = e^{-i(\omega_c-2\omega_p)t}\tilde{\varrho}_{21}, \tag{13a}$$

$$\hat{\varrho}_{32} = e^{i\omega_p t}\varrho_{32} = \tilde{\varrho}_{32}. \tag{13b}$$

One can see that at multiphoton resonance $\Delta=0\Leftrightarrow\omega_c=\omega_p/2$ [see Eq. (7)], the two reference frames denoted by $\hat{\varrho}_{ij}$ and $\tilde{\varrho}_{ij}$ coincide for the two coherences in Eq. (13), similar to the case of incoherent pumping. We will investigate the multiphoton resonance case further in Sec. III A 2.

We now proceed with the evaluation of the response coefficients. Keeping only terms oscillating in phase with the probe field, we arrive at

$$\tilde{\chi}_e = \frac{N}{\varepsilon_0\hbar}d_{32}^2\hat{\varrho}_{32}^{(0,1)}, \tag{14a}$$

$$\tilde{\chi}_m = \frac{N\mu_0}{\hbar}\mu_{21}^2\hat{\varrho}_{21}^{(1,0)}, \tag{14b}$$

$$\tilde{\xi}_{HE} = -i\frac{Nc\mu_0}{\hbar}d_{32}\mu_{21}e^{i\Phi}\hat{\varrho}_{21}^{(0,1)}, \tag{14c}$$

$$\tilde{\xi}_{EH} = i\frac{Nc\mu_0}{\hbar}d_{32}\mu_{21}e^{-i\Phi}\hat{\varrho}_{32}^{(1,0)}, \tag{14d}$$

where $\hat{\varrho}_{ij}^{(1,0)}$ and $\hat{\varrho}_{ij}^{(0,1)}$ are expansion coefficients in a Taylor series of $\hat{\varrho}_{ij}$ $(i,j\in\{1,2,3\})$ in terms of Ω_{32} and Ω_{21}:

$$\hat{\varrho}_{32} = \hat{\varrho}_{32}^{(0,0)} + \hat{\varrho}_{32}^{(0,1)}\Omega_{32} + \hat{\varrho}_{32}^{(1,0)}\Omega_{21} + O(\Omega_{21}^2,\Omega_{32}^2,\Omega_{21}\Omega_{32}), \tag{15a}$$

$$\hat{\varrho}_{21} = \hat{\varrho}_{21}^{(0,0)} + \hat{\varrho}_{21}^{(0,1)}\Omega_{32} + \hat{\varrho}_{21}^{(1,0)}\Omega_{21} + O(\Omega_{21}^2,\Omega_{32}^2,\Omega_{21}\Omega_{32}). \tag{15b}$$

In Eqs. (15), we call $\hat{\varrho}_{32}^{(0,1)}\Omega_{32}$ and $\hat{\varrho}_{21}^{(1,0)}\Omega_{21}$ the "direct terms," since they correspond to the susceptibilities, while $\hat{\varrho}_{32}^{(1,0)}\Omega_{21}$ and $\hat{\varrho}_{21}^{(0,1)}\Omega_{32}$ are denoted "cross terms" as they give rise to the chiralities. Also, in Eqs. (14), we have introduced the relative phase

$$\Phi = \phi_{32} - \phi_{21} \tag{16}$$

between the scalar dipole moments, which we write as

$$\vec{d}_{32}\vec{e}_p = d_{32}e^{i\phi_{32}}, \tag{17}$$

$$\vec{\mu}_{21}\vec{b}_p = \mu_{21}e^{i\phi_{21}}. \tag{18}$$

Equations (14) give the desired relation between the density matrix elements and the coefficients that determine the magnetic response. These can now be used in Eqs. (11) in order to determine the contribution of the various processes to the polarization and magnetization. Keeping only the terms relevant to the probe field response in phase with the probe field frequency, we find

$$\vec{P} = \frac{N}{\hbar}\vec{e}_p e^{i(\vec{k}_p\vec{r}-\omega_p t+\phi)}(d_{32}\mu_{21}\mathcal{B}_p e^{-i\Phi}\hat{\varrho}_{32}^{(1,0)} + d_{32}^2\mathcal{E}_p\hat{\varrho}_{32}^{(0,1)}) + \text{c.c.}, \tag{19a}$$

$$\vec{M} = \frac{N}{\hbar}\vec{b}_p e^{i(\vec{k}_p\vec{r}-\omega_p t+\phi)}(d_{32}\mu_{21}\mathcal{E}_p e^{i\Phi}\hat{\varrho}_{21}^{(0,1)} + \mu_{21}^2\mathcal{B}_p\hat{\varrho}_{21}^{(1,0)}) + \text{c.c.} \tag{19b}$$

III. ANALYTICAL RESULTS

We next solve the time-dependent equations of motion (5) for both our systems. First, we consider the closed-loop system for arbitrary multiphoton detuning Δ and derive an expression for the coherences to first order in the magnetic and electric probe field Rabi frequencies Ω_{21} and Ω_{32}. Then, we consider the special cases $\Delta \neq 0$ and $\Delta = 0$. Finally, we solve the incoherently pumped system.

A. Closed-loop system

The equations of motion for the closed-loop system are obtained from Eqs. (5), if we set $r_1 = 0$. We define the vector $\tilde{R}$ containing all density matrix elements,

$$\tilde{R} = (\tilde{\varrho}_{11}, \tilde{\varrho}_{12}, \tilde{\varrho}_{13}, \tilde{\varrho}_{21}, \tilde{\varrho}_{22}, \tilde{\varrho}_{23}, \tilde{\varrho}_{31}, \tilde{\varrho}_{32})^T. \tag{20}$$

The equations of motion (5) can be rewritten in terms of $\tilde{R}$ as

$$\frac{\partial}{\partial t}\tilde{R} = M\tilde{R} + \Sigma. \tag{21}$$

Here, we have eliminated $\tilde{\varrho}_{33}$ via the trace condition $\mathrm{Tr}(\tilde{\varrho}) = 1$, which is the reason for the appearance of the constant term Σ in Eq. (21). We proceed by splitting both M and $\tilde{R}$ up into terms with different time dependencies as follows:

$$M = M_0 + M_1\Omega_{21}e^{i\Delta t} + M_{-1}\Omega_{12}e^{-i\Delta t}, \tag{22}$$

$$\Sigma = \Sigma_0 + \Sigma_1\Omega_{21}e^{i\Delta t} + \Sigma_{-1}\Omega_{12}e^{-i\Delta t}, \tag{23}$$

where M_k and Σ_k $(k \in \{-1, 0, 1\})$ are time independent.

According to Floquet's theorem [34], the solution of $\tilde{R}$ has only contributions oscillating with frequencies that are integer multiples of Δ. Since terms oscillating at higher frequencies are suppressed by powers of the magnetic probe field Rabi frequency $|\Omega_{21}|$, we expand $\tilde{R}$ to first order in this Rabi frequency, and work with the ansatz

$$\tilde{R} = \tilde{R}_0 + \tilde{R}_1\Omega_{21}e^{i\Delta t} + \tilde{R}_{-1}\Omega_{12}e^{-i\Delta t} + O(|\Omega_{12}|^2). \tag{24}$$

From Eqs. (21)–(24), a comparison of coefficients yields

$$\tilde{R}_0 = -M_0^{-1}\Sigma_0, \tag{25a}$$

$$\tilde{R}_1 = -(M_0 - i\Delta)^{-1}(M_1\tilde{R}_0 + \Sigma_1), \tag{25b}$$

$$\tilde{R}_{-1} = -(M_0 + i\Delta)^{-1}(M_{-1}\tilde{R}_0 + \Sigma_{-1}). \tag{25c}$$

Since the density matrix element $\hat{\varrho}_{21}$ oscillating in phase with the probe field and $\tilde{\varrho}_{21}$ are related as

$$\hat{\varrho}_{21} = e^{-i(\omega_c-2\omega_p)t}\tilde{\varrho}_{21} = e^{-i(\omega_c-2\omega_p)t}(\tilde{R}_0)_4 + (\tilde{R}_1)_4\Omega_{21} + e^{-2i(\omega_c-2\omega_p)t}(\tilde{R}_{-1})_4\Omega_{12}, \tag{26}$$

one can determine $(\tilde{R}_1)_4$ as the part of $\hat{\varrho}_{21}$ oscillating in phase with the probe field, where the index 4 denotes the fourth component of $\tilde{R}_1$. Likewise, the relevant part of $\hat{\varrho}_{32}$ can be identified with $(\tilde{R}_0)_8$.

Note that $\tilde{R}_0$, $\tilde{R}_{-1}$, and $\tilde{R}_1$ are independent of Ω_{21}, but do depend on the electric probe field Rabi frequency Ω_{32}, which we did not take into account so far. Since we are interested in only the linear magnetic and electric response, we still have to expand the appropriate components of $\tilde{R}$ in Ω_{32}. We obtain

$$\hat{\varrho}_{21} = (\tilde{R}_1)_4\Omega_{21} + (\tilde{R}_0)_4 e^{-i(\omega_c-2\omega_p)t} + O(\Omega_{21}^2, \Omega_{32}^2, \Omega_{21}\Omega_{32}), \tag{27a}$$

$$\hat{\varrho}_{32} = (\tilde{R}_{-1})_8 e^{-i(\omega_c-2\omega_p)t}\Omega_{12} + (\tilde{R}_0)_8 + O(\Omega_{21}^2, \Omega_{32}^2, \Omega_{21}\Omega_{32}), \tag{27b}$$

where $(\tilde{R}_0)_4 \propto \Omega_{23}$ and $(\tilde{R}_0)_8 \propto \Omega_{32}$, and higher orders of Ω_{32} have been neglected. With Eqs. (25) and (27), an explicit evaluation yields

$$\begin{aligned}\hat{\varrho}_{21} = \frac{2}{B}\Bigg(&\frac{8\Delta_1^3\gamma_3 + 4i\Delta_1^2\gamma_3(2i\Delta_3 + \gamma_s) + \Delta_3[8|\Omega_{31}|^2(\gamma_2 - \gamma_3) - 2\Gamma]}{4|\Omega_{31}|^2 + (2\Delta_3 - i\gamma_3)(2\Delta_1 - 2\Delta_3 + i\gamma_s)} \\ &+ \frac{2\Delta_1[-4|\Omega_{31}|^2(\gamma_2 - 2\gamma_3) + \Gamma] - i[(4|\Omega_{31}|^2\gamma_2 - \Gamma)\gamma_s - 4|\Omega_{31}|^2\gamma_3^2]}{4|\Omega_{31}|^2 + (2\Delta_3 - i\gamma_3)(2\Delta_1 - 2\Delta_3 + i\gamma_s)}\Bigg)\Omega_{21} \\ &- \left(\frac{4}{B}\frac{4|\Omega_{31}|^2(\gamma_2 - \gamma_3) + [2\Delta_1 + i(\gamma_1 + \gamma_2)]\gamma_3(-2\Delta_2 - i\gamma_s)}{4|\Omega_{31}|^2 + [2i(\Delta_1 - \Delta_2) + \gamma_3](-2i\Delta_2 + \gamma_s)}\right)e^{-i(\omega_c-2\omega_p)t}\Omega_{31}\Omega_{23},\end{aligned} \tag{28a}$$

$$\begin{aligned}\hat{\varrho}_{32} = &\left(\frac{4}{B}\frac{4|\Omega_{31}|^2(-\gamma_2 + \gamma_3) + [2\Delta_1 + i(\gamma_1 + \gamma_2)]\gamma_3(2\Delta_1 - 2\Delta_3 - i\gamma_s)}{4|\Omega_{31}|^2 + (2\Delta_3 + i\gamma_3)(2\Delta_1 - 2\Delta_3 - i\gamma_s)}\right)e^{-i(\omega_c-2\omega_p)t}\Omega_{31}\Omega_{12} \\ &- \left(|\Omega_{31}|^2\frac{8}{B}\frac{[2(-\Delta_1 + \Delta_2)\gamma_2 + i\gamma_3(2i\Delta_2 + \gamma_1 + \gamma_3)]}{4|\Omega_{31}|^2 + (-2i\Delta_1 + 2i\Delta_2 + \gamma_3)(2i\Delta_2 + \gamma_s)}\right)\Omega_{32},\end{aligned} \tag{28b}$$

where

$$B = 4\Delta_1^2\gamma_3 + \Gamma + 4|\Omega_{31}|^2(\gamma_2 + 2\gamma_3), \tag{29a}$$

$$\gamma_s = \gamma_1 + \gamma_2 + \gamma_3, \tag{29b}$$

$$\Gamma = (\gamma_1 + \gamma_2)^2\gamma_3. \tag{29c}$$

Note that, in Eq. (28), the multiphoton detuning Δ has been replaced using Eq. (6). Also, the contributions without explicit time dependence via an exponential factor are the direct terms, while the other parts are cross terms.

1. Nonzero multiphoton detuning ($\Delta \neq 0$)

In the case of nonzero multiphoton detuning, $\Delta \neq 0 \Leftrightarrow 2\omega_p \neq \omega_c$, only the direct terms in Eqs. (28) oscillate in phase with the probe field. Therefore, only these terms contribute to the coherences and thus to the magnetic and electric responses. Then, the cross terms in Eqs. (14) vanish and therefore the chirality coefficients vanish, $\tilde{\xi}_{EH} = \tilde{\xi}_{HE} = 0$. This means that the polarization (magnetization) is entirely determined by the electric (magnetic) probe field component. It will turn out in Sec. III B that this case is comparable to the incoherently pumped system, in which there are no cross terms either.

2. Multiphoton resonance ($\Delta = 0$)

We now focus on the case of multiphoton resonance, i.e., $\Delta = 0$ or $\omega_p = \omega_c/2$. Hence, Eqs. (5) become time independent and we can now solve the linear system Eq. (21) for a time-independent steady-state solution of $\tilde{R}$ using $\frac{\partial}{\partial t}\tilde{R} = 0$. Now, all terms in Eq. (24) contribute, apart from terms that contain Ω_{32} in higher than first order. From Eqs. (13) we also find that the simplified relations between the two considered reference frames Eqs. (12) hold as in the case of incoherent driving.

We again neglect terms of higher order in the probe field Rabi frequency and arrive at

$$\begin{aligned}\hat{\varrho}_{21} = &-\frac{2i}{C_+ D}\{8i\Delta_2^3\gamma_3 + 4\Delta_2^2(4i\Delta_3 - \gamma_s)\gamma_3 - (4\Delta_3^2\gamma_3 + \Gamma)\gamma_s \\ &+ 4|\Omega_{31}|^2[\gamma_2(\gamma_1 + \gamma_2) + (2i\Delta_3 + \gamma_2)\gamma_3 - \gamma_3^2] \\ &+ 2i\Delta_2[-4|\Omega_{31}|^2(\gamma_2 - 2\gamma_3) + \Gamma \\ &+ 4\gamma_3\Delta_3(\Delta_3 + i\gamma_s)]\}\Omega_{21} - \frac{4\Omega_{31}}{C_+ D}\{4|\Omega_{31}|^2(\gamma_2 - \gamma_3) \\ &- [2(\Delta_2 + \Delta_3) + i(\gamma_1 + \gamma_2)]\gamma_3(2\Delta_2 + i\gamma_s)\}\Omega_{23},\end{aligned} \tag{30a}$$

$$\begin{aligned}\hat{\varrho}_{32} = &-\frac{4\Omega_{31}}{C_- D}\{4|\Omega_{31}|^2(\gamma_2 - \gamma_3) - [2(\Delta_2 + \Delta_3) \\ &+ i(\gamma_1 + \gamma_2)]\gamma_3(2\Delta_2 - i\gamma_s)\}\Omega_{12} \\ &- \frac{8i}{C_- D}|\Omega_{31}|^2[2i\Delta_3\gamma_2 + \gamma_3(2i\Delta_2 + \gamma_1 + \gamma_3)]\Omega_{32},\end{aligned} \tag{30b}$$

where

$$C_\pm = 4|\Omega_{31}|^2 + (\pm 2i\Delta_3 + \gamma_3)(\mp 2i\Delta_2 + \gamma_s), \tag{31a}$$

$$D = 4(\Delta_2 + \Delta_3)^2\gamma_3 + \Gamma + 4|\Omega_{31}|^2(\gamma_2 + 2\gamma_3), \tag{31b}$$

$$\Gamma = (\gamma_1 + \gamma_2)^2\gamma_3, \tag{31c}$$

$$\gamma_s = \gamma_1 + \gamma_2 + \gamma_3. \tag{31d}$$

The control field detuning Δ_1 has been eliminated using the relation $\Delta_1 = \Delta_2 + \Delta_3$ which follows from Eq. (6) in the case of $\Delta = 0$.

We see that both the direct terms and the cross terms contribute to the coherences and thus to the magnetic and electric response in this case. Therefore, the chirality coefficients are nonzero in the resonance case $\Delta = 0$, see Eqs. (14).

B. Incoherently pumped system

We now consider the electric and magnetic response in the incoherently pumped system shown in Fig. 1(b). It will serve us as a reference in a comparison to the results of the closed-loop system in order to determine the exact origin of the various contributions to the medium response.

In this system, the transformed Hamiltonian is time independent. Hence, we can solve for the steady-state solution just as in the case of multiphoton resonance in Sec. III A 2. The equations of motion follow from Eqs. (5) with $\Delta_1 = 0$ and $\Omega_{31} = \Omega_{13} = 0$. Instead of the coherent coupling field, they include an incoherent, bidirectional pump rate r_1 on transition $|1\rangle \leftrightarrow |3\rangle$.

Using Eqs. (12), up to first order in the probe field we find for the coherences in a reference frame oscillating in phase with the probe field:

$$\begin{aligned}\hat{\varrho}_{21} = &\frac{2i[r_1(\gamma_3 - \gamma_2) + (\gamma_1 + \gamma_2)\gamma_3]}{(2i\Delta_3 + r_1 + \gamma_3)[(\gamma_1 + \gamma_2)\gamma_3 + r_1(\gamma_2 + 2\gamma_3)]}\Omega_{21} \\ &+ O(\Omega_{21}^2, \Omega_{32}^2, \Omega_{21}\Omega_{32}),\end{aligned} \tag{32a}$$

$$\begin{aligned}\hat{\varrho}_{32} = &\frac{2ir_1(\gamma_2 - \gamma_3)}{(2i\Delta_2 + \gamma_s + r_1)[(\gamma_1 + \gamma_2)\gamma_3 + r_1(\gamma_2 + 2\gamma_3)]}\Omega_{32} \\ &+ O(\Omega_{21}^2, \Omega_{32}^2, \Omega_{21}\Omega_{32}).\end{aligned} \tag{32b}$$

In this case, the electric [magnetic] probe transition coherence is determined by the electric [magnetic] probe field component, and no cross terms appear.

IV. COMPARISON OF THE TWO SYSTEMS

We will now proceed with a comparison of the two systems. To this end, we will discuss the expansion coefficients $\hat{\varrho}_{32}^{(a,b)}$ and $\hat{\varrho}_{21}^{(a,b)}$ $(a,b \in \{0,1\})$ in Eqs. (15), since they determine the magnetic and electric responses according to Eqs. (19).

It will turn out that the direct terms are similar in many regards in both systems. These terms describe the establishment of polarization (magnetization) due to the electric (magnetic) probe field component. But crucial differences are found for the cross terms, which only appear in the

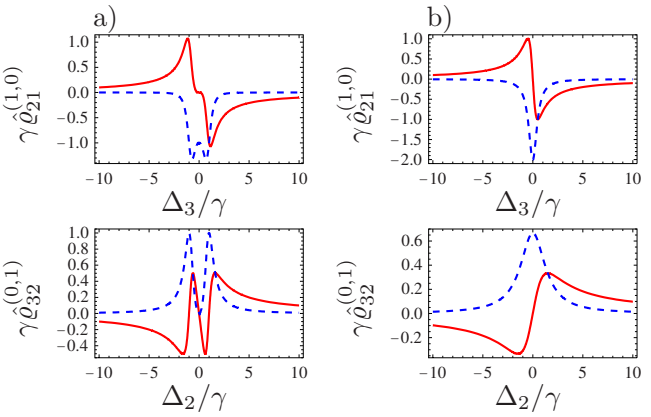

FIG. 2. (Color online) Real (red solid curve) and imaginary (blue dashed curve) parts of the direct terms in the magnetic and electric susceptibilities, respectively. The top row shows $\hat{\varrho}_{21}^{(1,0)}$, the bottom row $\hat{\varrho}_{32}^{(0,1)}$. (a) Closed-loop system and (b) incoherently pumped system as shown in Fig. 1.

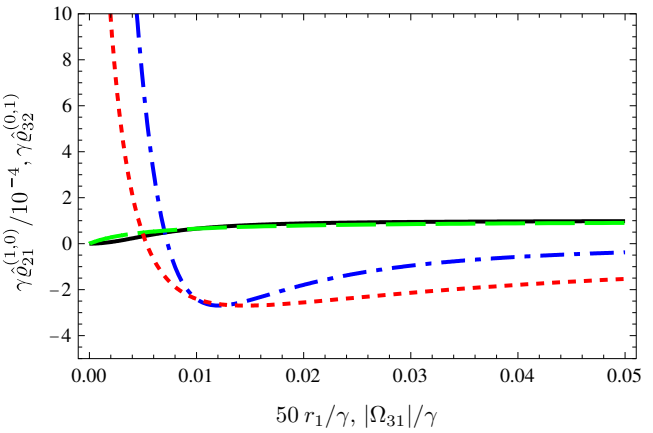

FIG. 3. (Color online) Dependence of the expansion coefficients $\hat{\varrho}_{32}^{(0,1)}$ in the closed loop (black solid line) and in the incoherently pumped system (green long-dashed line) as well as $\hat{\varrho}_{21}^{(1,0)}$ for the closed-loop (blue dash-dotted) and the incoherently pumped (red dashed) systems on the strength of the control field and the incoherent pump rate, respectively. Shown are only the imaginary parts of the coefficients evaluated at their absolute maxima. For the incoherent configuration, the maximum of $\mathrm{Im}(\hat{\varrho}_{21}^{(1,0)})$ is always at $\Delta_3=0$, and the maximum of $\mathrm{Im}(\hat{\varrho}_{32}^{(0,1)})$ is at $\Delta_2=0$. The coefficients are scaled by γ to obtain a unitless quantity and $\hat{\varrho}_{21}^{(1,0)}$ is scaled by a factor of 10^{-4}. In this figure, negative values indicate amplification, positive values absorption.

closed-loop system for zero multiphoton detuning. These terms characterize the polarization (magnetization) due to the magnetic (electric) probe field component.

A. The direct terms

From Secs. III A 1, III A 2, and III B it is clear that direct terms appear both in the loop system and in the system with incoherent pumping. In Fig. 2, the corresponding expansion coefficients for the two cases are compared. Since transitions $|1\rangle \leftrightarrow |2\rangle$ and $|1\rangle \leftrightarrow |3\rangle$ are electrically dipole allowed, whereas transition $|2\rangle \leftrightarrow |3\rangle$ is magnetically dipole allowed, we choose the decay rates as $\gamma_1=\gamma$, $\gamma_2=\gamma$, $\gamma_3=\alpha^2\gamma$. For the incoherent case, the pump rate is set to $r_1=\gamma$, whereas in the closed-loop configuration, the coherent pump field is set to $\Delta_1=0$, $\Omega_{31}=\gamma$. All expansion coefficients are plotted against the respective probe field detunings Δ_2 or Δ_3.

We find that in many respects, the direct terms of both systems behave similarly. Apart from the ac Stark splitting in the closed-loop system, the general structure is comparable and in particular the magnitude of the coefficients is of similar order in both systems.

The similarities become more apparent when considering the dependence of the direct terms on the coherent pump rate Ω_{31} and the incoherent pump rate r_1, as shown in Fig. 3. For this figure, the direct terms of the loop system are evaluated at a particular detuning Δ_2 or Δ_3, respectively, at which the absolute value of the imaginary part becomes maximal. At the same point, the real part vanishes. For the incoherently pumped system, the corresponding maxima always occur at $\Delta_3=0$ or $\Delta_2=0$, respectively. This approach allows to compare the two systems independently of the ac Stark splitting appearing in the closed-loop system only. Due to the growing splitting with increasing $|\Omega_{31}|$, a comparison at a fixed detuning would not be meaningful. It can be seen from Fig. 3 that both systems show a qualitatively similar dependence on the pumping strength. The shown imaginary part of the coherences characterizes the absorptive behavior of our systems: positive values stand for absorption and negative values for amplification of the magnetic or electric probe field component.

Interestingly, in both systems it is possible to choose the respective pump rate in such a way that $\hat{\varrho}_{21}$ vanishes at all frequencies. This is the case at the roots of the green long-dashed lines in Fig. 3. It turns out that, at these points, the populations of states $|1\rangle$ and $|2\rangle$ are the same such that the magnetic probe field component can traverse the medium without attenuation and without experiencing diffraction.

For the interpretation of Fig. 3, we calculate the coherences in terms of the (zeroth-order) populations for arbitrary detuning. In the case of incoherent pumping, we obtain

$$\hat{\varrho}_{21} = 2\Omega_{21}\frac{\hat{\varrho}_{11}^{(0)} - \hat{\varrho}_{22}^{(0)}}{2\Delta_3 - i(r_1 + \gamma_3)}, \tag{33a}$$

$$\hat{\varrho}_{32} = 2\Omega_{32}\frac{\hat{\varrho}_{22}^{(0)} - \hat{\varrho}_{33}^{(0)}}{2\Delta_2 - i(r_1 + \gamma_1 + \gamma_2 + \gamma_3)}. \tag{33b}$$

The zeroth-order populations are

$$\hat{\varrho}_{11}^{(0)} = \frac{(r_1 + \gamma_1 + \gamma_2)\gamma_3}{C}, \tag{34a}$$

$$\hat{\varrho}_{22}^{(0)} = \frac{r_1\gamma_2}{C}, \tag{34b}$$

$$\hat{\varrho}_{33}^{(0)} = \frac{r_1\gamma_3}{C}, \tag{34c}$$

where $C=r_1\gamma_2+2r_1\gamma_3+\gamma_1\gamma_3+\gamma_2\gamma_3$.

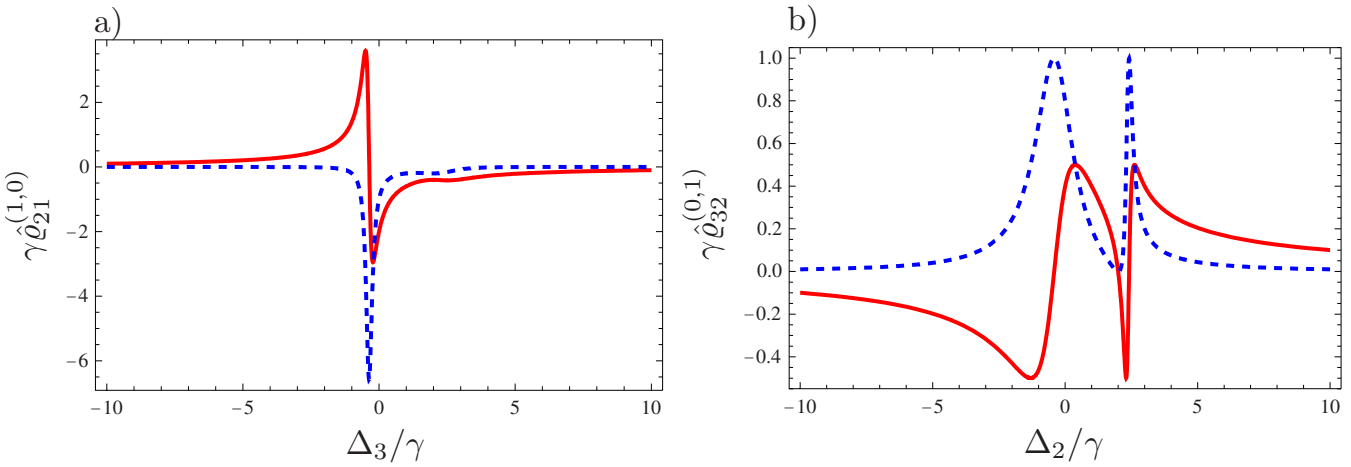

FIG. 4. (Color online) Real (red solid line) and imaginary (blue dashed curve) parts of the expansion coefficients (a) $\hat{\varrho}_{21}^{(1,0)}$ and (b) $\hat{\varrho}_{32}^{(0,1)}$ in Eqs. (15). The curves are drawn for $\Delta_1=2\gamma$ in the closed-loop system. The coefficients are scaled by γ. The parameters are as in Fig. 2(a), except for the nonvanishing detuning of the control field.

Note that in our system $\gamma_3 \ll \gamma_2$ due to the different multipolarity of the transitions. Therefore, for small pump rates r_1, from Eqs. (34) one finds $\hat{\varrho}_{11}^{(0)} > \hat{\varrho}_{22}^{(0)} > \hat{\varrho}_{33}^{(0)}$. As a result, both probe transitions are absorptive—although for $\hat{\varrho}_{21}$ only in a very small range of r_1 as compared to γ.

For large r_1, Eqs. (34) show that $\hat{\varrho}_{11}^{(0)} < \hat{\varrho}_{22}^{(0)}$ and $\hat{\varrho}_{33}^{(0)} < \hat{\varrho}_{22}^{(0)}$. In fact, $\hat{\varrho}_{11}^{(0)} \approx \hat{\varrho}_{33}^{(0)}$ for $r_1 \gg \gamma$. Hence, the magnetic probe transition becomes amplifying, whereas the electric transition maintains its absorptive character. As expected, from Eqs. (33), it follows directly that a population inversion causes amplification.

As a side note, we would like to mention the fact that Eqs. (33) imply vanishing $\hat{\varrho}_{32}$ for $\gamma_2=\gamma_3$. This is due to the fact that from Eqs. (34), one then finds $\hat{\varrho}_{22}^{(0)}=\hat{\varrho}_{33}^{(0)}$. However, this case is not of relevance for the current analysis, since $\gamma_3 \ll \gamma_2$.

Let us now examine the behavior of the closed-loop system with regard to a change of $|\Omega_{31}|$. In this case, the coherences are given by

$$\hat{\varrho}_{21} = 2\Omega_{21}\frac{K_1(\hat{\varrho}_{22}^{(0)} - \hat{\varrho}_{11}^{(0)}) + 4|\Omega_{31}|^2(\hat{\varrho}_{33}^{(0)} - \hat{\varrho}_{11}^{(0)})}{(4|\Omega_{31}|^2 + K_2)K_3}, \tag{35a}$$

$$\hat{\varrho}_{32} = 2\Omega_{32}\frac{K_4(\hat{\varrho}_{33}^{(0)} - \hat{\varrho}_{22}^{(0)}) + 4|\Omega_{31}|^2(\hat{\varrho}_{33}^{(0)} - \hat{\varrho}_{11}^{(0)})}{(4|\Omega_{31}|^2 + K_5)K_3}, \tag{35b}$$

while the populations obey

$$\hat{\varrho}_{11}^{(0)} = \frac{\gamma_3(K_6 + 4|\Omega_{31}|^2)}{K_7 + 4\gamma_2|\Omega_{31}|^2 + 8\gamma_3|\Omega_{31}|^2}, \tag{36a}$$

$$\hat{\varrho}_{22}^{(0)} = \frac{4\gamma_2|\Omega_{31}|^2}{K_7 + 4\gamma_2|\Omega_{31}|^2 + 8\gamma_3|\Omega_{31}|^2}, \tag{36b}$$

$$\hat{\varrho}_{33}^{(0)} = \frac{4\gamma_3|\Omega_{31}|^2}{K_7 + 4\gamma_2|\Omega_{31}|^2 + 8\gamma_3|\Omega_{31}|^2} \tag{36c}$$

where the K_l, $(l \in \{1,\ldots 7\})$ are coefficients independent of Ω_{31}.

Again, the coherence $\hat{\varrho}_{ij}$ is determined by the difference of the populations of $\hat{\varrho}_{ii}^{(0)}$ and $\hat{\varrho}_{jj}^{(0)}$ $[(i,j) \in \{(2,1),(3,2)\}]$. For small $|\Omega_{31}|$, the term proportional to $\hat{\varrho}_{33}^{(0)} - \hat{\varrho}_{11}^{(0)}$ can be neglected. For large $|\Omega_{31}|$, this term outweighs the others at first sight. However, for $|\Omega_{31}| \to \infty$ and arbitrary, but fixed detunings, one finds

$$\hat{\varrho}_{11}^{(0)} \to \frac{1}{\gamma_2/\gamma_3 + 2}, \tag{37a}$$

$$\hat{\varrho}_{22}^{(0)} \to \frac{1}{2\gamma_3/\gamma_2 + 1}, \tag{37b}$$

$$\hat{\varrho}_{33}^{(0)} \to \frac{1}{\gamma_2/\gamma_3 + 2}. \tag{37c}$$

Therefore, $\hat{\varrho}_{11}^{(0)} - \hat{\varrho}_{33}^{(0)} \to 0$ such that also in this case, $\hat{\varrho}_{ij}$ is determined by $\hat{\varrho}_{ii}^{(0)} - \hat{\varrho}_{jj}^{(0)}$.

Equations (37) also imply that for a strong control field, both probe transitions show opposite absorptive behavior (see Fig. 3): absorption in case of the upper probe transition, and amplification for the lower one. The reason is that due to the small decay rate γ_3, most population is trapped in state $|2\rangle$, such that the relevant population differences in Eqs. (35) have opposite sign. For small $|\Omega_{31}|$, Eqs. (36) yield $\hat{\varrho}_{11}^{(0)} > \hat{\varrho}_{22}^{(0)} > \hat{\varrho}_{33}^{(0)}$, which explains the absorptive properties in Fig. 3.

Before we come to the discussion of the cross terms, we would like to note that, of course, there are also differences between the direct terms of the two systems. We already discussed the ac Stark shift that occurs only in the loop system. But the closed-loop system also offers more degrees of freedom than the incoherently pumped system, most impor-

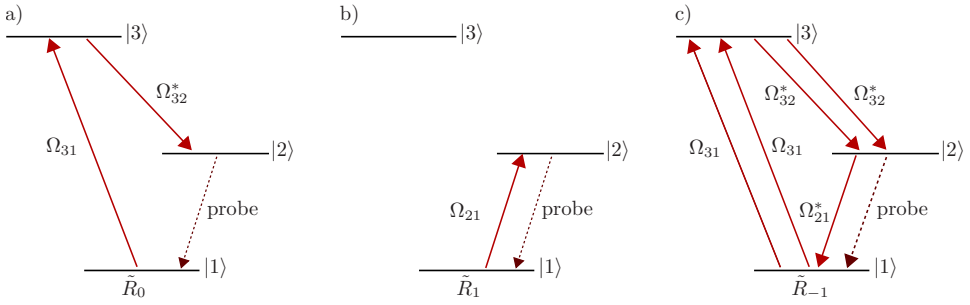

FIG. 5. (Color online) Interpretation of the different scattering processes that contribute to $\tilde{\varrho}_{21}$ in the case of $\Delta=0$. (a) $\tilde{R}_0$ contributes to the cross term in $\tilde{\varrho}_{21}$, and thus to the chirality $\tilde{\xi}_{HE}$. (b) $\tilde{R}_1$ contributes to the direct term, i.e., to the magnetic susceptibility. (c) $\tilde{R}_{-1}$ is of higher order in either one of the probe field Rabi frequencies and therefore negligible in our calculation.

tantly Δ_1. The role of the control field detuning Δ_1 is shown in Fig. 4. In this figure, we plot the expansion coefficients of the direct terms in the coherence over the probe field detunings Δ_2 and Δ_3 for $\Delta_1=2\gamma$. The detuning Δ_1 essentially determines the position of one of the maxima of the imaginary part of the response function. Increasing Δ_1 moves the peak to higher frequencies, while decreasing it moves it to lower frequencies. For example, in Fig. 4, the corresponding maximum can be seen close to $\Delta_2=2\gamma$.

B. The cross terms

Let us now come to the most important difference between the two systems: The coherences of the closed-loop system have cross terms, while the coherences of the incoherently pumped system do not. However, as found in Sec. III A, the cross terms contribute only to the magnetic and electric responses for $\Delta=0$, i.e., for $\omega_p=\omega_c/2$. The following comparison serves as basis for the conclusion which will be drawn in the discussion section regarding the enhancement of the magnetic response.

The mathematical origin of the cross terms can be identified from the derivation of the coherences in Sec. III A. The relevant response of the system to the probe field is given by the contributions of the respective probe transition coherences oscillating in phase with the incident probe field. According to this criterion, for $\Delta\neq 0$, only one of the terms in Eq. (24) contributes to each probe field coherence. In contrast, for $\Delta=0$, all terms in Eq. (24) contribute to this response. The additional terms lead to the cross terms discussed here. In principle, also other terms contribute in this case, but they are of higher order in the probe field Rabi frequencies and can therefore be neglected in linear response theory.

How can we interpret the different contributions $\tilde{R}_k$ ($k\in\{-1,0,1\}$) to Eq. (24) physically? An explicit calculation reveals their dependence on the probe and control field Rabi frequencies. The control field Rabi frequencies appear for two different reasons. First, the populations depend on the control field Rabi frequencies. But second, the Rabi frequencies also indicate the physical process described by the respective terms. The obtained combinations of the different Rabi frequencies lead to an interpretation of $\tilde{R}_k$ as depicted in Figs. 5 and 6. For example, $\tilde{R}_0$ contributing to $\tilde{\varrho}_{21}$ is shown in Fig. 5(a). This term arises from the scattering of the control field off of transition $|1\rangle\rightarrow|3\rangle$ and the probe field off of transition $|3\rangle\rightarrow|2\rangle$ into the probe transition $|2\rangle\rightarrow|1\rangle$, which contributes to the magnetic response.

We now turn to a numerical study of the cross terms. In Fig. 7, we plot $\hat{\varrho}_{21}^{(0,1)}$, multiplied by a factor of γ to achieve unitless quantities. $\hat{\varrho}_{32}^{(1,0)}$ is not shown, as it is virtually identical to $-\hat{\varrho}_{21}^{(0,1)}$ for the chosen parameters. It is important to note that, in Fig. 7, the cross terms are plotted over the variable σ which is defined as $\sigma=\frac{1}{2}(\Delta_3-\Delta_2)=\omega_2-\frac{1}{2}(\omega_3+\omega_1)$. This new variable can be interpreted as the energy shift of state $|2\rangle$ with respect to the average energy of $|1\rangle$ and $|3\rangle$. Hence, in a plot against σ, effectively state $|2\rangle$ is moved. In this way, the probe field frequency remains fixed such that the multiphoton resonance condition $\Delta=0\Leftrightarrow\omega_p=\omega_c/2$ is satisfied for all values of σ. For $\sigma=0$, $|2\rangle$ lies in the very middle of $|1\rangle$ and $|3\rangle$.

It turns out that apart from the phases of the dipole moments, the chiralities in Eqs. (14) depend on the phase $\psi-2\phi+\vec{K}\vec{r}$ arising from the closed interaction loop, where $\vec{K}=(\vec{k}_c-2\vec{k}_p)$ is the so-called wave vector mismatch. For the plot in Fig. 7, we set all involved phases to zero. This does not affect our final conclusion regarding the enhancement of the magnetic response, since it will only be based on the magnitude of the cross terms. If in an experiment the difference between the absolute field phases $\psi-2\phi$ is not fixed, then the chiralities average to zero. While absolute phase control is very difficult to achieve, relative phase control has been accomplished experimentally [22]. In related systems, the phase dependence of the cross terms can be made independent of the probe field phase, as will be discussed in Sec. V. The observed phase dependence is a characteristic of closed-loop systems, and has been observed in related systems as well [15,30]. The phase can be calculated by following the interaction loop, and counting phases of fields that deexcite the atom and phases of fields that excite the atom throughout this loop path with opposite sign.

Due to the dependence of the chiralities on $\vec{K}\vec{r}$, a further condition for the enhancement arises, namely, that the so-called wave vector mismatch should vanish, i.e., $\vec{K}=\vec{0}$. This condition on the relative propagation directions of the different fields for the enhancement to take place can be fulfilled, for example, for copropagating fields [30].

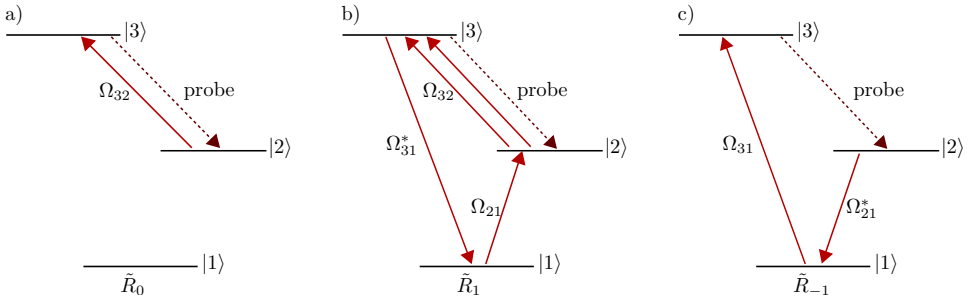

FIG. 6. (Color online) Interpretation of the different scattering processes that contribute to $\tilde{\varrho}_{32}$ in the case of $\Delta=0$. (a) $\tilde{R}_0$ contributes to the direct term in $\tilde{\varrho}_{32}$, and thus to the electric susceptibility. (b) $\tilde{R}_1$ is of higher order in either one of the probe field Rabi frequencies and can therefore be neglected. (c) $\tilde{R}_{-1}$ contributes to one of the cross terms, i.e., to one of the chirality coefficients.

C. Parametric enhancement of the magnetic response

We are now in the position to evaluate the magnitude of the magnetic response. For this, we examine the different contributions in Eq. (19b). In particular, we compare the two contributions to the magnetization, which except for the common prefactor are given by

$$M_1 = d_{32}\mu_{21}\mathcal{E}_p e^{i\Phi}\hat{\varrho}_{21}^{(0,1)}, \tag{38a}$$

$$M_2 = \mu_{21}^2\mathcal{B}_p\hat{\varrho}_{21}^{(1,0)}. \tag{38b}$$

Here, M_1 refers to the cross-term contribution that only contributes at $\Delta=0$ and M_2 denotes the direct term.

First, Figs. 2 and 7 show that in the closed-loop system

$$|\hat{\varrho}_{21}^{(1,0)}| \approx |\hat{\varrho}_{21}^{(0,1)}|. \tag{39}$$

Thus, the magnitude of the two expansion coefficients is comparable. Note that in Sec. IV D we will show that a further optimization allows to significantly enhance the chiral response. The order of magnitude of the involved transition dipole moments can be estimated as

$$\mu_{21} \sim \mu_B \sim ea_0\alpha c, \tag{40a}$$

$$d_{32} \sim ea_0, \tag{40b}$$

where μ_B is the Bohr magneton, e the elementary charge, a_0 the Bohr radius, α the fine-structure constant, and c the vacuum speed of light. Finally,

$$\mathcal{B}_p = \frac{1}{c}\mathcal{E}_p. \tag{41}$$

With Eqs. (40) and (41), we thus arrive at

$$|M_1| \approx \alpha^{-1}|M_2|. \tag{42}$$

Therefore at multiphoton resonance, the magnetic response of the closed-loop system is enhanced by a factor of α^{-1} due to the scattering of the electric probe field component into the magnetic probe transition (described by $\tilde{R}_0$ in Fig. 5). This explains the chiral enhancement observed in previous proposals for achieving negative refraction in atomic gases, and concludes our analysis of the origin of the parametric enhancement. A similar argument shows that the direct terms of the incoherently pumped and the closed loop system are comparable in magnitude, such that the closed-loop system in multiphoton resonance also allows an enhancement of the magnetic response by α^{-1} as compared to the incoherently pumped system.

D. Nonparametric enhancement of the magnetic response

In the previous section, we have identified the mechanism that led to a parametric enhancement by α^{-1} of the magnetic response. This mechanism was used in recent proposals to realize negative refraction in a dense gas [12–15]. It is important to note, however, that there is the as-yet unexplored additional possibility to enhance the magnetic response nonparametrically via the expansion coefficient $\hat{\varrho}_{21}^{(0,1)}$ in Eq. (38). In the following, we show that our system allows to achieve a considerable further nonparametric enhancement of the magnetic response via an optimization of this coefficient.

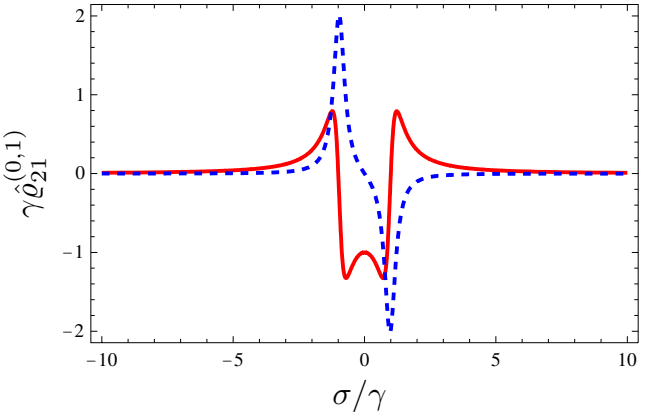

FIG. 7. (Color online) Real (red solid line) and imaginary (blue dashed) parts of the expansion coefficient $\hat{\varrho}_{21}^{(0,1)}$ in the closed-loop system [see Eqs. (15)]. $\hat{\varrho}_{32}^{(1,0)}$ is not shown, since it is virtually identical to $-\hat{\varrho}_{21}^{(0,1)}$. The coefficients correspond to cross terms and determine $\tilde{\xi}_{HE}$ and $\tilde{\xi}_{EH}$, respectively. The plotted coefficients are phase dependent; in this figure all phases are set to zero. The variable $\sigma=(\Delta_3-\Delta_2)/2=\omega_2-(\omega_3+\omega_1)/2$ denotes the shift of the eigenfrequency of $|2\rangle$ with respect to the average frequency of $|1\rangle$ and $|3\rangle$. Then, for all values of σ, the multiphoton resonance condition $\Delta=0$ is satisfied for a fixed probe field frequency ω_p.

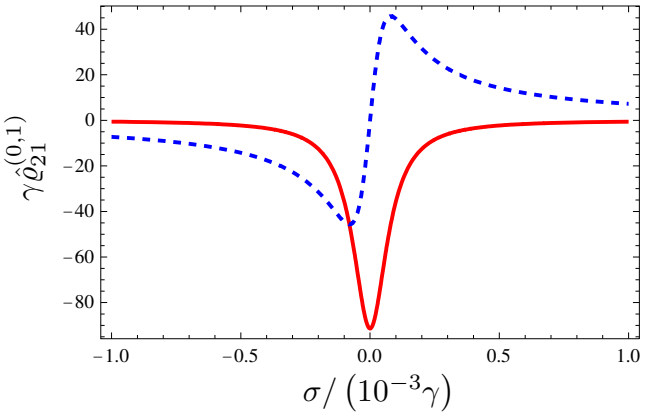

FIG. 8. (Color online) Nonparametric enhancement of the magnetic response. The parameters are as in Fig. 7, but with $\Omega_{31}=\alpha\gamma$. Note the different scale of the frequency axis.

To this end, we reconsider the expression for the chiral contribution to the magnetization, $\hat{\varrho}_{21}^{(0,1)}$ [see Eq. (19)]. From Eqs. (15) and (26), we find that we need to optimize $(R_0)_4$. Again, we consider parameters $\gamma_1=\gamma$, $\gamma_2=\gamma$, $\gamma_3=\alpha^2\gamma$, and set the phases to zero. An expansion with respect to the small parameter α then yields

$$\gamma\hat{\varrho}_{21}^{(0,1)}=\frac{\gamma\Omega_{31}}{(\Delta_2-\Delta_1)(\Delta_2+i\gamma)-|\Omega_{31}|^2}+O(\alpha^2). \quad (43)$$

Choosing $\Delta_2=\Delta_1$, this expression reduces to

$$\gamma\hat{\varrho}_{21}^{(0,1)}=-\frac{\gamma}{\Omega_{13}}. \quad (44)$$

This means that for this particular probe field frequency the chiral contribution can be made very large by choosing a small Ω_{13}, albeit only over a small range of σ since the peak structure is very narrow (see Fig. 8). In this figure, the parameters are $\Delta_1=0$, and $\Omega_{31}=\alpha\gamma$. Also, Fig. 8 shows the result to all orders of α.

The special importance of pumping strengths $|\Omega_{31}|\sim\alpha\gamma$ becomes clear if one analyzes the three populations. For $|\Omega_{31}|<\alpha\gamma$, most population is trapped in $|1\rangle$, because the weak pumping $|1\rangle\rightarrow|3\rangle$ limits the population dynamics. But if $|\Omega_{31}|>\alpha\gamma$, then most population is trapped in $|2\rangle$ due to the small natural decay rate out of $|2\rangle$. Close to the critical value $\alpha\gamma$, the populations of $|1\rangle$ and $|2\rangle$ both are close to 0.5, such that a maximum coherence on the magnetic probe transition can be created. A comparison with the direct response terms shows that it is indeed the chiral contribution that dominates the magnetic response in this parameter range. The narrow width of the peak structure arises from the two-photon resonance of the transition $|1\rangle\rightarrow|2\rangle$ induced by the control field and the electric probe field component.

It should be noted that for all values of σ, the multiphoton resonance condition is fulfilled in Fig. 8. This is possible, since the parameter $\sigma=(\Delta_3-\Delta_2)/2$ only determines the eigenfrequency of state $|2\rangle$ with respect to the states $|1\rangle$ and $|3\rangle$. Also, the small width of the peak structure in Fig. 8 does not impose additional constraints on the system, since the non-parametric enhancement is also possible if the level structure is such that state $|2\rangle$ is not exactly in the middle between $|1\rangle$ and $|3\rangle$, i.e., for $\sigma\neq0$. From Eq. (43), we require $\Delta_1=\Delta_2$ to achieve maximum enhancement. This together with the multiphoton resonance condition $\Delta=\Delta_2+\Delta_3-\Delta_1=0$ implies $\Delta_3=0$. Thus, the nonparametric enhancement occurs at $\sigma=-\Delta_1/2+\mathcal{O}(\alpha^2)$, and therefore can be adjusted via Δ_1. The contributions of higher order in α, however, cause the peak to decrease in height for $\Delta_1\neq0$. For $\Delta_1=\gamma$, the minimum of the real part has a value of $\gamma\,\mathrm{Re}(\hat{\varrho}_{21}^{(0,1)})\approx-52$.

From Fig. 8, we also see that for the chosen value of $\Omega_{31}=\alpha\gamma$, Eqs. (43) and (44) do not quantitatively predict the exact maximum value of the response, since corrections of order α^2 become important. Nevertheless, from Fig. 8 which was plotted without any of the approximations leading to Eq. (44), we find that $\gamma\,\mathrm{Re}(\hat{\varrho}_{21}^{(0,1)})\approx-91$, i.e., a nonparametric enhancement almost of order α^{-1}. Thus, we have shown that a suitable optimization of the control laser fields allows to considerably enhance the magnetic response in addition to the parametric enhancement by α^{-1} discussed in Sec. IV C.

A similar calculation for the chiral contribution to the electric polarization yields

$$\gamma\hat{\varrho}_{32}^{(1,0)}=\frac{\gamma\Omega_{31}}{\Delta_3(i\gamma-\Delta_2)-|\Omega_{31}|^2}+O(\alpha^2). \quad (45)$$

Choosing $\Delta_3=0$, this expression simplifies to

$$\gamma\hat{\varrho}_{32}^{(1,0)}=-\frac{\gamma}{\Omega_{13}}. \quad (46)$$

As discussed above, at multiphoton resonance, the condition $\Delta_2=\Delta_1$ required to optimize the chiral contribution to the magnetic response Eq. (43) is equivalent to $\Delta_3=0$. Therefore, from Eq. (45) we find that both chiral contributions can be nonparametrically enhanced at the same time by choosing $\Delta_3=0$.

V. DISCUSSION

We have seen that the direct response, which describes the polarization (magnetization) created by the electric (magnetic) probe field component, is of the same order of magnitude in all three cases considered in Sec. III. Only at multiphoton resonance does the response of the closed-loop system contain in addition a term corresponding to the scattering of the electric probe field component into the magnetic probe field transition. We showed that this scattering effectively enhances the magnetic response by one inverse power of the fine-structure constant α^{-1}, and thus identified this scattering as the origin of the chiral enhancement facilitated in current proposals for negative refraction in atomic gases.

Of course, the reverse process of scattering the magnetic field into the electric probe field mode can also occur. However, Eqs. (19) show that this does not lead to an enhancement of the electric response, since, mathematically speaking, $|d_{32}^2\vec{E}_p|\sim\alpha^{-1}|d_{32}\mu_{32}\vec{B}_p|$. Physically speaking, the coupling of the magnetic probe field component to a magnetic transition is smaller than the coupling of the electric probe field component to an electric transition by a factor of α.

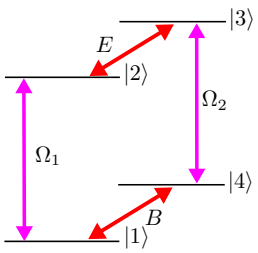

FIG. 9. (Color online) Example level scheme for magnetic response enhancement independent of the probe field frequency. Ω_1 and Ω_2 are coherent coupling fields with frequencies ω_1 and ω_2, respectively. E and B are the electric and magnetic components of the probe field with frequency ω_p. Here, the closed-loop path contains an absorption and an emission of a probe field photon such that the multiphoton detuning $\Delta=\omega_1-\omega_2$ can be satisfied for arbitrary probe field frequencies.

The multiphoton resonance condition restricts the magnetic enhancement in the system discussed here to a single probe field frequency. Extended closed-loop systems can be constructed in such a way that a complete loop contains an excitation on the electric probe transition and a deexcitation on the magnetic probe transition, or vice versa [14,15]. A simple example for this is shown in Fig. 9. In such a system, the multiphoton resonance condition does not depend on the frequency of the probe field, such that it can be satisfied for arbitrary probe field frequencies by suitably choosing the coupling field frequencies. The physical interpretation identified in our analysis directly carries over to these extended systems. It should be noted, however, that the multiphoton resonance condition goes along with similar conditions on the wave vectors of the coupling and probe fields that need to be fulfilled in order to obtain chiral enhancement, as discussed in Sec. IV B. This is of particular importance if the level structure does not allow to achieve low absorption both for the coupling and the probe fields. Then, a pencil-shaped medium could be used, where the weakly absorbed probe field propagates along the long axis of the medium, whereas the more strongly absorbed control fields propagate along the small axis of the medium. Such extended geometries are restricted by the fact that chiral enhancement occurs only if the wave vector mismatch is zero.

The analysis of different level schemes has shown that, even with the chiral parametric enhancement by α^{-1}, very dense gases with particle densities of order 10^{17} cm^{-3} are required in order to achieve sufficient magnetic response. But our results show that further nonparametric enhancements of similar magnitude as the parametric enhancements are possible. Ideally, parametric and nonparametric enhancement should be combined, enabling one to further relax the requirement for a high vapor density. Alternatively, a nonparametric enhancement can be used to increase the direct magnetic response term, such that no chiral contributions to the magnetic response are required. This could lead to a relaxation of the stringent conditions on the atomic level scheme that needs to contain an electric dipole and a magnetic dipole transition with similar transition frequency for the chiral enhancement to take place. One example could be two-component gases, where one atomic species accounts for the electric response, whereas the other species leads to magnetic response [35], similar to the case in metamaterials.

In conclusion, by using a time-dependent analysis and by comparing a chiral closed-loop system to a reference system, we have identified the mechanism leading to the parametric chiral enhancement of the magnetic response by a factor of α^{-1}. This enhancement can be traced back to a multiphoton scattering of the electric probe field component into the magnetic probe field component. We have further shown that our system in addition to this parametric enhancement allows the magnetic response to be nonparametrically increased by almost two orders of magnitude via a suitable choice of the control field parameters. A combination of parametric and nonparametric response could lead to negative refraction at substantially lower vapor densities.

[1] V. G. Veselago, Sov. Phys. Usp. **10**, 509 (1968).
[2] V. Veselago, L. Braginsky, V. Shkliver, and C. Hafner, J. Comput. Theor. Nanosci. **3**, 189 (2006).
[3] V. M. Shalaev, Nat. Photonics **1**, 41 (2007).
[4] D. R. Smith, J. B. Pendry, and M. C. K. Wiltshire, Science **305**, 788 (2004).
[5] J. B. Pendry, Phys. Rev. Lett. **85**, 3966 (2000).
[6] R. A. Shelby, D. R. Smith, and S. Schultz, Science **292**, 77 (2001).
[7] E. Cubukcu, K. Aydin, E. Ozbay, S. Foteinopoulou, and C. M. Soukoulis, Nature (London) **423**, 604 (2003).
[8] A. A. Houck, J. B. Brock, and I. L. Chuang, Phys. Rev. Lett. **90**, 137401 (2003).
[9] A. Grbic and G. V. Eleftheriades, Phys. Rev. Lett. **92**, 117403 (2004).
[10] S. Zhang, W. Fan, N. C. Panoiu, K. J. Malloy, R. M. Osgood, and S. R. J. Brueck, Phys. Rev. Lett. **95**, 137404 (2005).
[11] C. M. Soukoulis, S. Linden, and M. Wegener, Science **315**, 47 (2007).
[12] M. O. Öktel and O. E. Müstecaplioglu, Phys. Rev. A **70**, 053806 (2004).
[13] Q. Thommen and P. Mandel, Phys. Rev. Lett. **96**, 053601 (2006).
[14] J. Kästel, M. Fleischhauer, S. F. Yelin, and R. L. Walsworth, Phys. Rev. Lett. **99**, 073602 (2007).
[15] P. P. Orth, J. Evers, and C. H. Keitel, e-print arXiv:0711.0303.
[16] M. Fleischhauer, C. H. Keitel, M. O. Scully, C. Su, B. T. Ulrich, and S.-Y. Zhu, Phys. Rev. A **46**, 1468 (1992).
[17] J. B. Pendry, Science **306**, 1353 (2004).
[18] S. J. Buckle, S. M. Barnett, P. L. Knight, M. A. Lauder, and D. T. Pegg, Opt. Acta **33**, 2473 (1986).
[19] D. V. Kosachiov, B. G. Matisov, and Y. V. Rozhdestvensky, J. Phys. B **25**, 2473 (1992).
[20] W. E. van der Veer, R. J. J. van Diest, A. Dönszelmann, and H. B. van Linden van den Heuvell, Phys. Rev. Lett. **70**, 3243 (1993).

[21] W. Maichen, F. Renzoni, I. Mazets, E. Korsunsky, and L. Windholz, Phys. Rev. A **53**, 3444 (1996).
[22] E. A. Korsunsky, N. Leinfellner, A. Huss, S. Baluschev, and L. Windholz, Phys. Rev. A **59**, 2302 (1999).
[23] E. A. Korsunsky and D. V. Kosachiov, Phys. Rev. A **60**, 4996 (1999).
[24] A. J. Merriam, S. J. Sharpe, M. Shverdin, D. Manuszak, G. Y. Yin, and S. E. Harris, Phys. Rev. Lett. **84**, 5308 (2000).
[25] S. A. Babin, S. I. Kablukov, U. Hinze, E. Tiemann, and B. Wellegehausen, Opt. Lett. **26**, 81 (2001).
[26] G. Morigi, S. Franke-Arnold, and G.-L. Oppo, Phys. Rev. A **66**, 053409 (2002).
[27] A. F. Huss, R. Lammegger, C. Neureiter, E. A. Korsunsky, and L. Windholz, Phys. Rev. Lett. **93**, 223601 (2004).
[28] V. S. Malinovsky and I. R. Sola, Phys. Rev. Lett. **93**, 190502 (2004).
[29] H. Shpaisman, A. D. Wilson-Gordon, and H. Friedmann, Phys. Rev. A **71**, 043812 (2005).
[30] M. Mahmoudi and J. Evers, Phys. Rev. A **74**, 063827 (2006).
[31] S. Kajari-Schroder, G. Morigi, S. Franke-Arnold, and G.-L. Oppo, Phys. Rev. A **75**, 013816 (2007).
[32] J. D. Jackson, *Classical Electrodynamics* (Wiley, New York, 1998).
[33] M. O. Scully and M. S. Zubairy, *Quantum Optics* (Cambridge University Press, Cambridge, U. K. 1997).
[34] M. G. Floquet, Ann. Sci. Ec. Normale Super. **12**, 47 (1883).
[35] B. Jungnitsch and J. Evers (unpublished).